SLAC-PUB-9534
October 2002

On the Nature of MeV-blazars

M. Sikora, M. Błażejowski, R. Moderski

Nicolaus Copernicus Astronomical Center, Bartycka 18, 00-716 Warsaw, Poland

sikora@camk.edu.pl

and

G. M. Madejski

Stanford Linear Accelerator Center, 2575 Sand Hill Road, Menlo Park, CA 94025, USA

Received ______________; accepted ______________

Revised version May 15, 2002

*Work supported in part by Department of Energy Contract DE-AC03-76SF00515.

ABSTRACT

Broad-band spectra of the FSRQ (flat-spectrum-radio quasars) detected in the high energy gamma-ray band imply that there may be two types of such objects: those with steep gamma-ray spectra, hereafter called MeV-blazars, and those with flat gamma-ray spectra, GeV-blazars. We demonstrate that this difference can be explained in the context of the ERC (external-radiation-Compton) model using the same electron injection function. A satisfactory unification is reachable, provided that: (a) spectra of GeV-blazars are produced by internal shocks formed at the distances where cooling of relativistic electrons in a jet is dominated by Comptonization of broad emission lines, whereas spectra of MeV-blazars are produced at the distances where cooling of relativistic electrons is dominated by Comptonization of near-IR radiation from hot dust; (b) electrons are accelerated via a two step process and their injection function takes the form of a double power-law, with the break corresponding to the threshold energy for the diffusive shock acceleration. Direct predictions of our model are that, on average, variability time scales of the MeV-blazars should be longer than variability time scales of the GeV-blazars, and that both types of the blazar phenomenon can appear in the same object.

Subject headings: galaxies: quasars: general — galaxies: jets — radiation mechanisms: nonthermal — gamma rays: theory — X-rays: general

1. INTRODUCTION

The data obtained from the Compton Gamma-ray Observatory (CGRO) mission suggest that blazars – the subclass of AGNs which includes FSRQ and BL Lac objects –

are strong γ–ray emitters (von Montigny et al. 1995; Mukherjee et al. 1997). In these objects γ–ray radiation forms a distinctive spectral component, clearly separated from another, lower energy component, presumably produced by the synchrotron process. As it was demonstrated by Fossati et al. (1998), blazar spectra form a sequence which can be parametrized by their total luminosity. In this sequence, FSRQs are the most luminous objects. Both their low and high energy spectral components appear to be the least extended to their respective high energies, and their γ–ray luminosity during flares strongly dominate over the luminosity of the synchrotron component. The least luminous blazars are represented by the X–ray selected BL Lac objects, often called HBLs (High-energy peaked BL Lacs). Their low energy spectral component extends up to hard X–rays, and their γ–ray spectrum reaches TeV energies. γ–ray flux detected in the TeV-emitting BL Lac objects usually does not dominate over synchrotron flux.

As predicted already in 1978 by Blandford and Rees and later supported by many independent observations and theoretical analyses, blazar radiation is most likely produced by nonthermal plasma in relativistic jets and Doppler boosted in our direction. Due to this, the Doppler enhancement of the jet renders the thermal components of the nucleus such as the UV radiation from an accretion disc, the X–ray radiation from the disc corona, and the infrared radiation from the hot dust – all presumably emitted isotropically – significantly diluted. But, at least in FSRQs, the optical-UV broad emission lines (BEL) are clearly detectable. They provide information about the redshift as well as the energetics of the central engine and about radiative environment of the sub-parsec/parsec scale jets. It turns out that the energy density of the BEL region on sub-parsec/parsec scales as measured in the comoving frame of the jet usually dominates the energy density of the synchrotron radiation. Within the framework of the internal shock model for the generation of radiative outbursts, that implies that the 1 – 10 day time scale γ–ray flares are produced by Comptonization of emission lines (external-radiation Compton [ERC] model) (Sikora, Begelman, & Rees 1994), rather than by Comptonization of synchrotron radiation (synchrotron-self-Compton [SSC] model), the latter presumably dominating the γ–ray production in the low luminosity BL Lac objects.

The ERC model successfully predicts the observed location of the spectral break in the high energy spectra of FSRQs to be in the 1 – 30 MeV range without the necessity of postulating a break in the power-law electron injection function. According to the model, this spectral break simply reflects the break in the electron energy distribution caused by the effect of particle cooling (Błażejowski et al. 2000; Sikora et al. 2001; see also §2). If this interpretation is correct, the change of the spectral slope around the break resulting from cooling should be unique and equal to $\Delta\alpha_{x\gamma} = 0.5$, where $\alpha : F_\nu \propto \nu^{-\alpha}$. In most FSRQs, $\Delta\alpha_{x\gamma} \leq 0.5$, and the values of $\Delta\alpha_{x\gamma}$ lower than 0.5 can be explained by invoking the possible dominant contribution of the SSC process in the soft/mid X-ray band. However, the so-called MeV-blazars present a challenge for the model. Their X-ray spectra are very hard, $\alpha_x = 0.3 - 0.5$, and the high-energy γ–ray spectra are very soft, $\alpha_\gamma > 1.4$, and, therefore, $\Delta\alpha_{x\gamma} \geq 1$ (Blom et al. 1998; Bloemen et al. 1995; Tavecchio et al. 2000). There were several attempts to explain such spectra in terms of the ERC model. Sikora et al. (1997) proposed an inhomogeneous model, according to which the X-ray spectra are due to superposition of multiple ERC components produced at different distances in a jet and having low energy spectral cutoffs at frequencies determined by the plasma temperature, assumed to increase with a distance. This model, however, cannot reproduce the correlation of the X-ray and γ–ray light curves during the 1996 February flare observed in 3C 279 (Wehrle et al. 1998; Lawson et al. 1999). Georganopoulos, Kirk, & Mastichiadis (2001) suggested that the steep γ–ray spectra can result from the fact that they are softened by the Klein-Nishina effect. But this effect is important in the EGRET band (30 MeV – 3 GeV) only if energy of the seed photons involved in the ERC process is more than 10 times greater than the typical energy of the BEL photons. Finally, Błażejowski et al. (2000)

demonstrated that soft γ–ray spectra can result from superposition of two components, one produced by Comptonization of BEL, and another due to Comptonization of near-IR radiation produced by hot dust. This model requires the high energy cutoff of the ERC(IR) component to be in the range 3 - 30 MeV and such a condition can be satisfied only via fine-tuning of the maximum electron energy to be within the range $3 \times 10^3 - 10^4\ m_e c^2$. Another weakness of this model is that the spectra superposed from the two components do not provide a good fit of the approximately power-law spectra observed in the EGRET band.

In the present work we assume that electrons are accelerated via a two-step process and that their injection function takes the form of a double power-law with a break at the energy which divides the regimes of dominance of two different acceleration mechanisms. Here the division energy is the threshold energy for the resonant scattering of electrons by Alfven waves (required to have efficient diffusive shock acceleration of electrons). With this, we demonstrate that the MeV-blazar type spectra are produced when γ–rays result from Comptonization of the infrared dust radiation, whereas the GeV-blazar type spectra are produced if the γ–ray flux is dominated by Comptonization of BEL. Our work is organized as follows: in §2, we discuss the cooling effect and demonstrate that for a distance range corresponding to the observed variability time scales, the cooling break is located within the 1 - 30 MeV range, as implied by observations. In §3, we discuss the issue of the electron acceleration efficiency and present the motivation for introducing the double power-law approximation for the electron injection function. Such an approximation is used in §4 to calculate the time-averaged spectra produced at different distances in a jet by shocks. There, we also demonstrate that adopting the same electron injection function, one can reproduce the typical spectra of both MeV- and GeV-blazars. Our results are summarized in §5.

2. ELECTROMAGNETIC SPECTRA

2.1. Cooling effect

The basic feature of the high energy spectra in FSRQs — a spectral break between the X–ray and the γ–ray bands — has a natural explanation in terms of the ERC model. In this model, X–ray spectra are produced by electrons with radiative cooling time scale t'_{cool}, longer than the source life-time t'_{fl} (*slow cooling regime*), whereas γ–rays are produced by electrons with $t'_{cool} < t'_{fl}$ (*fast cooling regime*). Noting that the angle-averaged cooling rate of electrons, when dominated by Comptonization of external radiation, is

$$|\dot{\gamma}| \simeq \frac{\sigma_T}{m_e c} u'_{ext} \gamma^2 \,, \tag{1}$$

where $\gamma \equiv E'_{el}/m_e c^2$ is the random Lorentz factor of the electron and u'_{ext} is the energy density of the diffuse external radiation field, both as measured in the source comoving frame, we obtain the angle-averaged cooling time scale of the electron to be

$$t'_{cool} \simeq \frac{\gamma}{|\dot{\gamma}|} \simeq \frac{m_e c}{\sigma_T} \frac{1}{\gamma u'_{ext}} \,, \tag{2}$$

where u'_{ext} is the energy density of an external radiation field. Then, from $t'_{cool} = t'_{fl} = \mathcal{D} t_{fl}$, where t_{fl} is the observed time scale of the flare, and

$$\mathcal{D} = \frac{1}{\Gamma(1 - \beta \cos\theta_{obs})} \tag{3}$$

is the bulk Lorentz factor, the break in the electron distribution is located at the energy

$$\gamma_c \simeq \frac{m_e c}{\sigma_T} \frac{1}{u'_{ext} t_{fl} \mathcal{D}} \,. \tag{4}$$

For $\gamma < \gamma_c$, the slope of the electron distribution is the same as the slope of the injection function; for $\gamma > \gamma_c$, the slope of the electron energy distribution is steeper by $\Delta s = 1$ ($s : N_\gamma \propto \gamma^{-s}$).

In the internal shock model, the lifetime of the flare is equal to the lifetime of the shock(s) and that is equal to the collision time scale of the two inhomogeneities, which prior to the collision are assumed to propagate down the jet with different velocities. Thus, we have the distance range where the shock is active to be

$$\Delta r_{coll} = ct_{fl}\mathcal{D}\Gamma \, , \tag{5}$$

and because time scales of flares in FSRQs are rarely shorter than 1 day, those flares are most likely produced at distances larger than 0.1 parsec. At such distances, the contribution to u'_{ext} is dominated by BEL and infrared radiation from hot dust. Noting that

$$u'_{ext} = \frac{1}{c}\int I'_{ext} d\Omega' = \frac{1}{c}\int I_{ext}\mathcal{D}_{in}^{-2} d\Omega \simeq u_{diff}\Gamma^2 \tag{6}$$

where

$$\mathcal{D}_{in} = \frac{1}{\Gamma(1-\beta\cos\theta_{in})} \tag{7}$$

and θ_{in} is the angle between the photon direction and the jet axis, we predict that the break in an electron energy distribution at γ_c should correspond to a break in the electromagnetic spectrum at frequency

$$\nu_c \simeq \mathcal{D}^2\gamma_c^2\nu_{diff} \simeq \left(\frac{m_e c}{\sigma_T}\right)^2 \frac{\nu_{diff}}{u'^2_{ext} t_{fl}^2} \simeq \left(\frac{m_e c^2}{\sigma_T}\right)^2 \frac{\nu_{diff}}{u_{diff}^2 \Delta r_{coll}^2} \left(\frac{\mathcal{D}}{\Gamma}\right)^2 \tag{8}$$

and that the spectrum should change the slope around ν_c by $\Delta\alpha_{x\gamma} \simeq 0.5$ ($\leftarrow \Delta s = 1$).

2.2. External radiation fields

Broad emission line region

According to the interpretation of the data obtained in many reverberation campaigns, production of broad emission lines in quasars is stratified and peaked around a distance (see, e.g., Peterson 1993; Kaspi 2000; Sulentic, Marziani & Dultzin-Hacyan 2000)

$$r_{BEL} \sim 3.0 \times 10^{17}\sqrt{L_{UV,46}}\text{cm} \tag{9}$$

Unfortunately, the detailed dependence of line luminosities on distance and geometry of the BEL region is poorly known. For our illustrative purposes we assume that the BEL region is spherical and that the fraction of the central UV radiation reprocessed into lines at a distance r is $\xi_{BEL}(r > r_{BEL}) \equiv \partial\xi_{BEL}/\partial \ln r \propto (r_{BEL}/r)^q$ and $\xi_{BEL}(r < r_{BEL}) = 0$. With that, the energy density of BEL field, as measured in the comoving frame of the radiating plasma, can be approximated by

$$u'_{BEL}(r) \sim \frac{L_{BEL}\Gamma^2}{4\pi c r_{BEL}^2} \frac{q}{1 + (r/r_{BEL})^{2+q}}\,, \tag{10}$$

where $L_{BEL} = \xi_{BEL} L_{UV}$ and $\xi_{BEL} = \int_{r_{BEL}}^{\infty} (\partial\xi_{BEL}/\partial r) dr$. Note that for $r > r_{BEL}$, the value of $u_{BEL}(r)$ is dominated by radiation coming from smaller distances, from around r_{BEL}. However, since this radiation is redshifted in the source frame, the contribution to $u'_{BEL}(r)$ is dominated by the fraction of $u_{BEL}(r)$ which is determined by broad emission lines produced at a distance r.

Hot dust

Evidence that hot dust is present in blazars is indirect. Infrared emission of hot dust is directly measured in quasars which are observed at larger angles to the jet axis than blazars. The ratio of the IR flux to the UV flux in these objects shows that the fraction of the UV radiation reprocessed by the dust into the infrared, i.e. the dust covering factor ξ_{IR}, is of the same order as ξ_{BEL} (Sanders et al. 1989). Dust is probably concentrated in molecular tori, but optical extinction suggests that its distribution in the normal direction to the equatorial plane doesn't have any sharp boundary (Baker 1997). One of the unknown aspects of dust in quasars is the minimal distance from the nucleus where it can exist. This distance can be limited by the maximum temperature that dust can survive,

$$r_{d,min} \sim \frac{1}{T_{d,max}^2} \left(\frac{L_{UV}}{4\pi\sigma_{SB}} \right)^{1/2} \tag{11}$$

where $T_{d,max} \sim 1500$K, or by the inner edge of the torus if it is larger than $r_d(T_{d,max})$ (see, e.g., Yi, Field, & Blackman 1994). As observations of individual objects show, there is a very large scatter in the dust amount and its distance distribution amongst various quasars (Polletta et al. 2000; Andreani et al. 2002).

In the present calculations we approximate the dust distribution by assuming that it is spherical and enclosed within a given distance range with a constant covering factor. With these assumptions the energy density due to dust, as measured in the source comoving frame, can be estimated using the formula

$$u'_{IR}(r) \sim \frac{L_{d,IR}\Gamma^2}{4\pi c r_{d,min}^2} \frac{1}{1+(r/r_{d,min})^2} \frac{1}{\Lambda}, \tag{12}$$

where $\Lambda = \ln(r_{d,max}/r_{d,min}) \sim 5$. The dependence of u'_{UV} and u'_{IR} on r is illustrated in Fig. 1. For such radiation fields we plot the dependence of γ_c on r on Fig. 2 and of ν_c on r Fig. 3. It is apparent from the Fig. 3 that for a very wide range of r, the break $h\nu_c$ is located within the photon energy range 1 MeV – 30 MeV, in agreement with observations.

2.3. Electron injection function

As it was demonstrated by Sikora & Madejski (2000), the energy flux in powerful jets in quasars cannot be dominated by pair plasma. This is because such a jet would produce much larger flux of soft X–ray radiation than is observed. Hence, we assume that the inertia of the jet is dominated by protons. In this case, the structure of shocks and the structure of Alfven waves generated around the shocks are both determined by protons. Being resonantly scattered by these waves, the protons jump back and forth across the shock front and participate in the 1st order Fermi acceleration process (Bell 1978; Blandford & Ostriker 1978). Those protons which reach energies $> 10^9$ GeV interact efficiently with ambient photons and trigger (mainly via photo-meson process) synchrotron-supported pair cascades (Mannheim & Biermann 1992). However, such a model fails to reproduce the very hard X–ray spectra of FSRQs (Sikora & Madejski 2000). This may indicate that in the context of those models, too few protons reach sufficiently high energies to power pair cascades.

An alternative possibility is that the high energy radiation in FSRQs is produced by directly accelerated electrons. However, for efficient acceleration of electrons by the Fermi process via resonant scattering off Alfven waves, the electrons must be first preheated/preaccelerated up to energies γ_F, at which point the magnetic rigidity of electrons becomes comparable with magnetic rigidity of thermal protons, i.e. when their momenta are equal:

$$m_e\sqrt{\gamma_F^2 - 1} \simeq m_p\sqrt{\gamma_{p,th}^2 - 1}\,, \tag{13}$$

where

$$\gamma_{p,th} - 1 = \eta_{p,th}\kappa \tag{14}$$

is the average thermal proton energy in the shocked plasma, κ is the amount of energy dissipated per proton in units of m_pc^2, and $\eta_{p,th}$ is the fraction of the dissipated energy tapped to heat the protons. In the case of the two intrinsically identical inhomogeneities (Sikora & Madejski 2001)

$$\kappa \simeq \frac{((\Gamma_2/\Gamma_1)^{1/2} - 1)^2}{2(\Gamma_2/\Gamma_1)^{1/2}}\,. \tag{15}$$

where $\Gamma_2 > \Gamma_1 \gg 1$ are bulk Lorentz factors of inhomogeneities prior to the collision. For the reasonable assumption that $\Gamma_2/\Gamma_1 < 10$, the thermal proton plasma is at most mildly relativistic, i.e. $\gamma_{p,th} - 1 < 1$.

Noting that

$$n_e m_e(\bar{\gamma}_{inj} - 1) \simeq n_p m_p \eta_e \kappa = n_p m_p \frac{\eta_e}{\eta_{p,th}}(\gamma_{p,th} - 1)\,, \tag{16}$$

where $\bar{\gamma}_{inj}$ is the average Lorentz factor of injected electrons and η_e is the fraction of the dissipated energy used to accelerate electrons, we find that for γ_F and $\bar{\gamma}_{inj} \gg 1$

$$\frac{\gamma_F}{\bar{\gamma}_{inj}} \sim \frac{n_e}{n_p}\frac{\eta_{p,th}}{\eta_e}\left(\frac{\gamma_{p,th} + 1}{\gamma_{p,th} - 1}\right)^{1/2}\,. \tag{17}$$

Hence, for non- or mildly relativistic shocks and for $\eta_{p,th} \sim \eta_e$, the threshold energy for the diffusive shock acceleration of electrons significantly exceeds the average energy of electrons, even if $n_e = n_p$. This implies that the often-considered bulk preheating process is not able to provide an adequate number of electrons with $\gamma \geq \gamma_F$. However, as it was recently demonstrated in numerical PIC (particle-in-cell) simulations, the preheating/preacceleration mechanism can have a stochastic character and a non-negligible fraction of electrons can reach such energies (Dieckmann et al. 2000; Shimada & Hoshino 2000). Furthermore, the fact that even in blazars with the hardest X-ray spectra, the X-ray spectral indices α_X are always greater than 0 indicates that the largest number of electrons is injected at low energies, and, therefore, that there is no evidence for a bulk preheating process forcing most of electrons into equipartition with protons. This strongly suggests that in a similarity to the diffusive shock acceleration operating at $\gamma > \gamma_F$, the preacceleration process also has stochastic character and injects electrons with a power-law energy distribution. Motivated by this, we assume that electrons, being accelerated by the two-step process, are injected with the double power-law energy distribution

$$Q = \begin{cases} C_l \gamma^{-p_l} & \text{if } \gamma < \gamma_F \\ C_h \gamma^{-p_h} & \text{if } \gamma > \gamma_F \end{cases} , \tag{18}$$

where $C_h = C_l \gamma_F^{p_h - p_l}$. The injection break at γ_F given by Eqs. (13) - (15) results in a break in the electromagnetic spectrum at the frequency

$$\nu_F \simeq \mathcal{D}^2 \gamma_F^2 \nu_{diff} \, . \tag{19}$$

3. MeV-BLAZARS vs. GeV-BLAZARS

For $2 < \Gamma_2/\Gamma_1 < 10$ and $1/3 \leq \eta_{p,th} \leq 1/2$, the break in the electron injection function is $\gamma_F \sim 10^3$ (see Eqs. 13 - 15 and Fig. 2). Another break appears in the electron energy distribution at γ_c (Eq. 4). If the cooling of electrons is dominated by Comptonization of BEL, then $\gamma_c \ll \gamma_F$, and the frequency range $[\nu_c, \nu_F]$ overlaps significantly with the EGRET band. Hence, the spectrum in the EGRET band should show a slope $\alpha \sim p_l/2$ and should be steeper there than in the X-ray band by ~ 0.5 (or less, if the contribution of the SSC radiation into X-ray band is taken into account). For $p_l \leq 2.0$ such spectra become representative for short term flares in GeV-blazars (Pohl et al. 1997).

At larger distances, the production of γ–rays is dominated by Comptonization of infrared radiation of hot dust. Luminosity of that radiation is comparable or even larger than the luminosity of the broad emission line light, but because of greater distance, its energy density is much smaller than energy density of the diffuse radiation in the BEL region. As a consequence, the cooling break energy, γ_c, is now much larger, approaching the value comparable to the value of γ_F (see Fig. 2). Hence, there is no longer an extended spectral plateau with $\alpha = p_l/2$, and both ν_c and ν_F conspire to produce the spectral break $\Delta\alpha_{x\gamma} = 0.5 + (p_h - p_l)/2$. Since now the energy of the Comptonized diffuse photons is ν_{IR}/ν_{BEL} times lower than in the BEL region, an approximate location of this break is at a frequency which is by that factor lower than ν_F in the BEL region. Hence, the spectra produced in the EGRET band at larger distances are predicted to have a spectral slope $\simeq \alpha_3 = p_h/2$. For $p_l \leq 2.0$ and $p_h \geq 2.4$ such spectra become representative for MeV-blazars (Tavecchio et al. 2000).

The above scheme can also explain two other observed differences between MeV-blazars and GeV-blazars. One is that the X–ray spectra are generally much harder in MeV-blazars. In the context of the scenario above, this presumably results from the lower contribution of the SSC component to the X–ray band in the MeV-blazars than in the GeV-blazars, which is the case, e.g., if $(u'_{IR}/u'_B)_{r_2} > (u'_{BEL}/u'_B)_{r_2}$, where u'_B is the magnetic energy density and $r_2 \gg r_1 \sim r_{BEL}$. The other difference is that in the spectra of MeV-blazars, in contrast to GeV-blazars, the thermal UV bumps are quite prominent (Tavecchio et al. 2000). This difference can be explained by noting that magnetic fields are weaker at larger distances, and therefore in MeV-blazars, the synchrotron spectra are shifted to lower frequencies, revealing the UV bump. All of the above effects are illustrated in Figs. 4 & 5, where we present the time averaged spectra of radiation produced at two different distances by electrons injected with the same energy distribution, Q, given by Eq. (18). The spectra are computed using the internal shock model where the shock propagates down the conical jet, and including the following dominant radiation processes: synchrotron radiation – SYN; Comptonization of synchrotron radiation – SSC; Comptonization of BELs – ERC(BEL); and Comptonization of infrared radiation of hot dust – ERC(IR). The model is presented in Błażejowski et al. (2000) and Sikora et al. (2001); for a more comprehensive description of the model see Moderski et al., in preparation. The model input parameters used to calculate the presented spectra are specified in the figure captions.

In order to illustrate the relative location of the breaks at γ_c and γ_F in these two specific models, we present in Figs. 6 and 7 the energy distributions of electrons. They are computed at a distance of the shock termination (which in our models is at $r = 2r_0$) and presented together with the electron injection function to demonstrate the cooling effect.

It should be emphasized here that the value of γ_F does not depend on how the fraction $(1 - \eta_{p,th})$ of the energy dissipated in the shock is shared by other consistuents than thermal protons (see Eqs. 13 – 15). We also note that the comparison of the FSRQ spectra during outbursts against the spectra calculated from our model indicates that the best matching is provided by the models where the electron energy density exceeds the magnetic energy density by a factor ranging from a few up to more than 10.

4. CONCLUSIONS

We demonstrated that the appearance of a FSRQ as a GeV-blazar or a MeV-blazar can be explained as depending on the distance of the maximum rate of energy dissipation in a jet. The GeV-flat spectra are predicted by our scenario to originate at distances where the production of γ–rays is dominated by Comptonization of BEL, while the spectra characteristic of MeV-blazars are predicted to originate at distances where the production of γ–rays is dominated by Comptonization of hot dust radiation. An additional ingredient, required to reach satisfactory unification between these objects, is the assumption that electrons are injected with the double power-law energy distribution, with the break at $\gamma \sim 10^3$. Such location of the break coincides numerically with the threshold energy for the diffusive shock acceleration of electrons. Below that energy, the electrons must be accelerated by a different mechanism, e.g. following instabilities driven by shock-reflected ions (Hoshino et al. 1992; McClements et al. 1997; Shimada & Hoshino 2000; Dieckmann et al. 2000); or following reconnection of magnetic fields (Romanova & Lovelace 1992; Blackman 1996).

As observations of X-ray spectra in MeV-blazars show, less energetic relativistic electrons are accelerated with the power-law energy distribution, with index $p_l \leq 2$. Future studies of dependence of the spectral shape on time scales of outbursts can be used to verify our idea that spectral breaks $\Delta\alpha_{x\gamma} > 1$ result from superposition of two breaks, one produced by the cooling effect and another one reflecting the break in the electron injection function at the threshold energy for the Fermi acceleration process.

It is very likely that some of the MeV-blazar phenomena can be produced at distances where the source is already optically thin at mm-wavelengths. If this is the case, the model predicts a correlation between variability of the flux around the synchrotron-self-absorption break at mm-wavelengths and in the γ–ray band, on typical time scales of a month. This possibility is supported by recent polarization measurements at very high radio frequencies. Those observations reveal that magnetic field in the very compact radio cores is dominated by its prependicular component and this is consistent with the model of the radiation produced *in situ* by transverse shocks (Lister 2001). Depending on the amount and covering factor of the hot dust in the surrounding medium, such shocks can be sites of the MeV-peaked γ–ray blazars.

Finally, we would like to comment that the MeV-blazar and GeV-blazar phenomena can interchangeably appear within the same object, as likely is the case in PKS 0208-512 (Stacy et al. 1996; Blom et al. 1996). With such objects, correlation between the spectral type and the variability time scales can be studied directly, without the bias introduced, for instance, by the dependence of the variability time scales on the black hole mass which can be very different from object to object. We note that the future sensitive γ–ray telescopes such as GLAST will provide us with excellent spectrally resolved light curves and will significantly constrain the applicability of radiative and particle acceleration models for those enigmatic sources.

This project was partially supported by Polish KBN grant 5 P03D 002 21 and a Chandra grant from NASA to Stanford University via the SAO award no. GO0-1038A. M.S. thanks SLAC for its hospitality during the completion of part of this work.

REFERENCES

Andreani, P., Fosbury, R.A.E., van Bemmel, I., & Freudling, W. 2002, A&A, 381, 389

Baker, J.C. 1997, MNRAS, 286, 23

Bell, A.R. 1978, MNRAS, 187, 142

Blackman, E.G. 1996, ApJ 456, L87

Blandford, R.D., & Ostriker, J.P. 1978, ApJ, 227, L49

Blandford, R.D., & Rees, M.J. 1978, in Pittsburgh Conf. on BL Lac Objects, ed. A.M. Wolfe (Pitthsburgh: Univ. Pittsburgh Press), 328

Błażejowski, M., Sikora, M., Moderski, R., & Madejski, G.M. 2000, ApJ, 545, 107

Bloemen, H., et al. 1995, A&A, 293, L1

Blom, J.J., et al. 1995, A&A, 295, 330

Blom, J.J., et al. 1996, A&AS, 120, 507

Dieckmann, M.E., McClements, K.G., Chapman, S.C., Dendy, R.O., & Drury, L.O'C. 2000, A&A, 356, 377

Fossati, G., Maraschi, L., Celotti, A., Comastri, A., & Ghisellini, G. 1998, MNRAS, 299, 433

Georganopoulos, M., Kirk, J.G., & Mastichiadis, A. 2001, ApJ, 561, 111

Hoshino, A., Arons, J., Gallant, Y.A., & Langdon, A.B. 1992, ApJ, 390, 454

Kaspi, S. 2000, in ASP Conf. Proc. 224, Probing the Physics of Active Galactic Nuclei, eds. B.M. Peterson, R.W. Pogge, & R.S. Polidan (San Francisco: Astronomical Society of the Pacific), 347

Lawson, A.J., McHardy, I.M., & Marscher, A.P. 1999, MNRAS, 306, 247

Lister, M.L. 2001, ApJ, 562, 208

Mannheim, K., & Biermann, P.L. 1992, A&A, 253,, L21

McClements, K.G., Dendy, R.O., Bingham, R., Kirk, J.G., & Drury, L.O'C. 1997, MNRAS, 291, 241

Mukherjee, R., et al. 1997, ApJ, 490, 116

Peterson, B.M. 1993, PASP, 105, 247

Pohl M., et al. 1997, A&A, 326, 51

Polletta, M., Courvoisier, T.J.-L., Hooper, E.J., & Wilkes, B.J. 2000, A&A, 362, 75

Romanova, M.M., & Lovelace, R.V.E. 1992, A&A, 262, 26

Sanders, D.B. et al. 1989, ApJ,347, 29

Shimada, N., & Hoshino, M. 2000, ApJ, 543, L67

Sikora, M., Begelman, M.C., & Rees, M.J. 1994, ApJ, 421, 153

Sikora, M., Błażejowski, M., Begelman, M.C., & Moderski, R. 2001, ApJ, 554, 1

Sikora, M., & Madejski, G.M. 2000, ApJ, 534, 109

Sikora, M., & Madejski, G.M. 2001, in AIP Conf. Proc. 558, High Energy Gamma-Ray Astronomy, ed. F.A. Aharonian & H.J. Völk (Melville, New York: AIP), 275

Sikora, M., & Madejski, G.M. 2001, preprint (astro-ph/0112231)

Sikora, M., Madejski, G., Moderski, R., & Poutanen, J. 1997, ApJ, 484, 108

Stacy J.G., et al. 1996, A&A Suppl.Ser.120, 549

Sulentic, J.W., Marziani, P., & Dultzin-Hacyan, D. 2000, ARA&A, 38, 521

Tavecchio F., et al. 2000, ApJ, 544, L23

von Montigny, C., et al. 1995, ApJ, 440, 525

Wehrle, A.E., et al. 1998, ApJ, 497, 178

Yi, I., Field, G.B., & Blackman, E.G. 1994, ApJ, 432, L31

This manuscript was prepared with the AAS LATEX macros v5.0.

FIGURE CAPTIONS

Fig. 1.— The dependence of the energy densities of external radiation fields, u'_{BEL} (dashed line) and u'_{IR} (solid line), and of energy density of magnetic field, $u'_B = B'^2/8\pi$ (dotted line) on the distance from the central source, r. The curves are calculated using Eqs. (10) and (12) for: $r_{BEL} = 5.2 \times 10^{17}$ cm; $r_{d,min} = 2.6 \times 10^{19}$ cm; $\Gamma = 15$; $L_{BEL} = 3.0 \times 10^{45}$ erg s^{-1}; $L_{d,IR} = 9.0 \times 10^{45}$ erg s^{-1}; $q = 1.0$; $\Lambda = 3.2$; and $B' = (1.2 \times 10^{18}\mathrm{cm}/r)$ Gauss.

Fig. 2.— The dependence of the electron energy distribution breaks, γ_c and γ_F, on distance. The γ_c curves are calculated using Eqs. (4) and (5) for $r = \Delta r_{coll}$: $\gamma_c(UV)$ (dashed line) – assuming that external radiation field is totally dominated by u'_{BEL}; and $\gamma_c(IR)$ (solid line) – assuming that external radiation field is totally dominated by u'_{IR}. The value of γ_F is obtained from Eqs. (13) – (15) for $\Gamma_2/\Gamma_1 = 3.0$ and $\eta_{p,th} = 0.5$. All other model parameters are the same as in Fig. 1.

Fig. 3.— The dependence of the "cooling break", ν_c on the distance from the central source r. The break is calculated for the same model parameters, as in previous figures and assuming $\theta_{obs} = 1/\Gamma$ ($\rightarrow \mathcal{D} = \Gamma$).

Fig. 4.— The model spectrum of the time averaged flare produced by the shock formed at a distance $r_0 = 6.0 \times 10^{17}$ cm and terminated at $r = 2r_0$. The shock propagates down the conical jet with a half-opening angle $\theta_j = 0.02$. The electrons/positrons are injected at the rate given by Eq. (18) for $C_l = 3 \times 10^{49}$ s^{-1}, $p_l = 1.8$, and $p_h = 2.8$. All other model parameters are the same as in previous figures. The two areas confined by vertical dashed lines represent the 2 – 10 keV and 30 MeV – 3 GeV bands, respectively. The sharp feature around $\nu \simeq \Gamma^2 \nu_{BEL}$ is the artifact of two approximations of our model: first, that we do not take into account upscattering of external photons produced at the distances smaller than the actual position of the shock in a jet – which would contribute to spectrum at $\nu < \Gamma^2 \nu_{BEL}$,

and second, that we use the average BEL frequency.

Fig. 5.— Same as Fig. 4, but for the shock formed at a distance $r_0 = 2.0 \times 10^{19}$ cm.

Fig. 6.— Energy distribution of electrons $\gamma^2 N_\gamma$ at $r = 2r_0$ for $r_0 = 6.0 \times 10^{17}$ cm, shown as a dotted line. For illustration, we also show the electron injection function multiplied by the period of the shock operation $\gamma^2 Q t'_{fl}$ as a solid line.

Fig. 7.— Same as Fig. 6, but for the shock formation distance $r_0 = 2.0 \times 10^{19}$ cm.

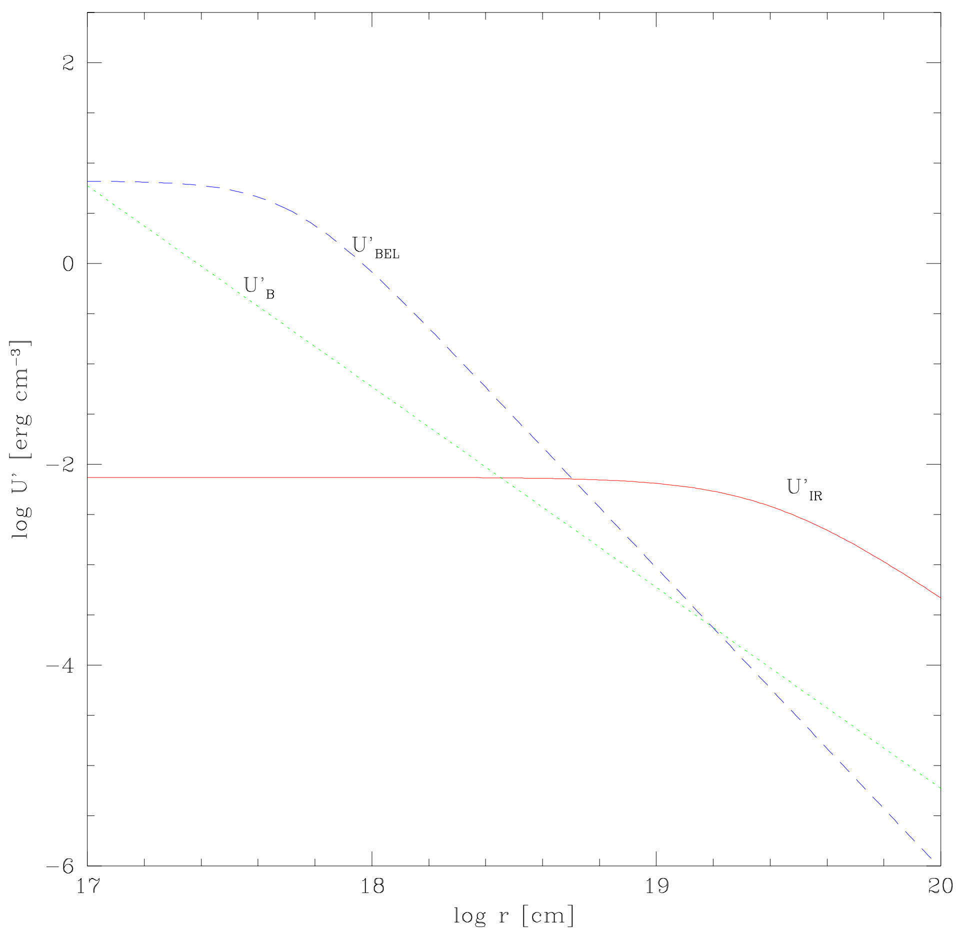
2
0
−2
−4
−6
17
18
19
20
log U' [erg cm⁻³]
log r [cm]
U'BEL
U'B
U'IR

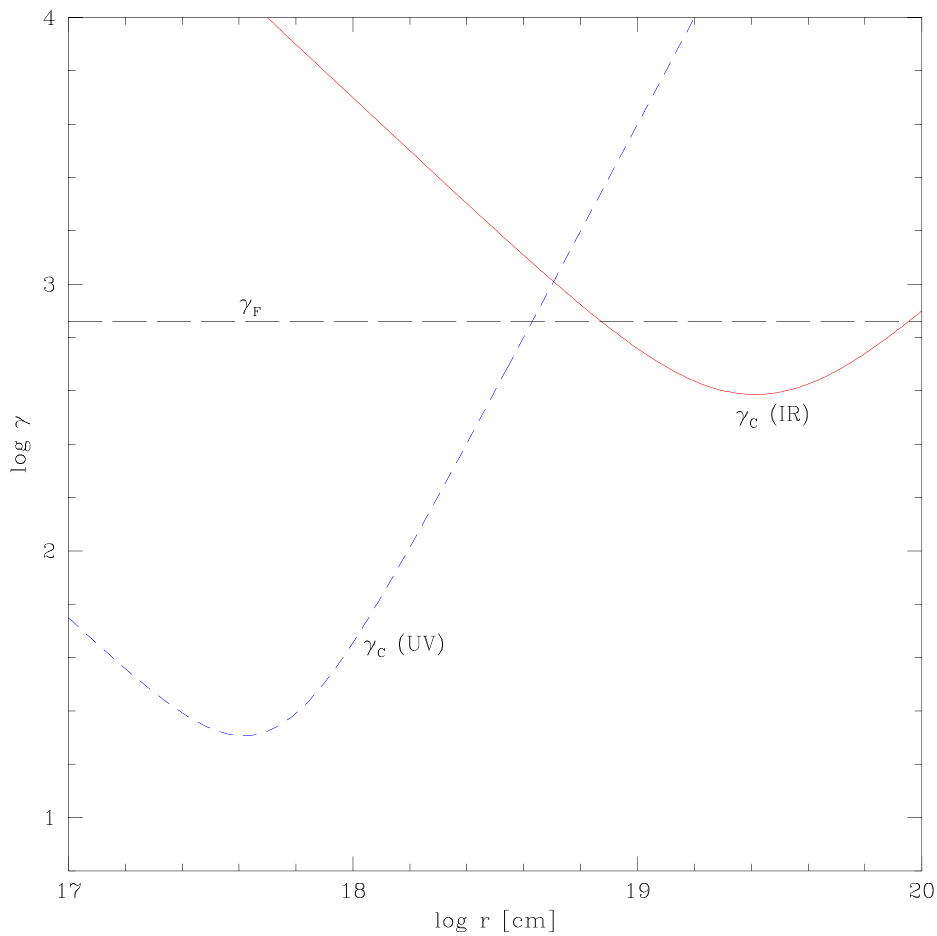

4
3
2
1
log γ
γ_F
γ_C (IR)
γ_C (UV)
17
18
19
20
log r [cm]

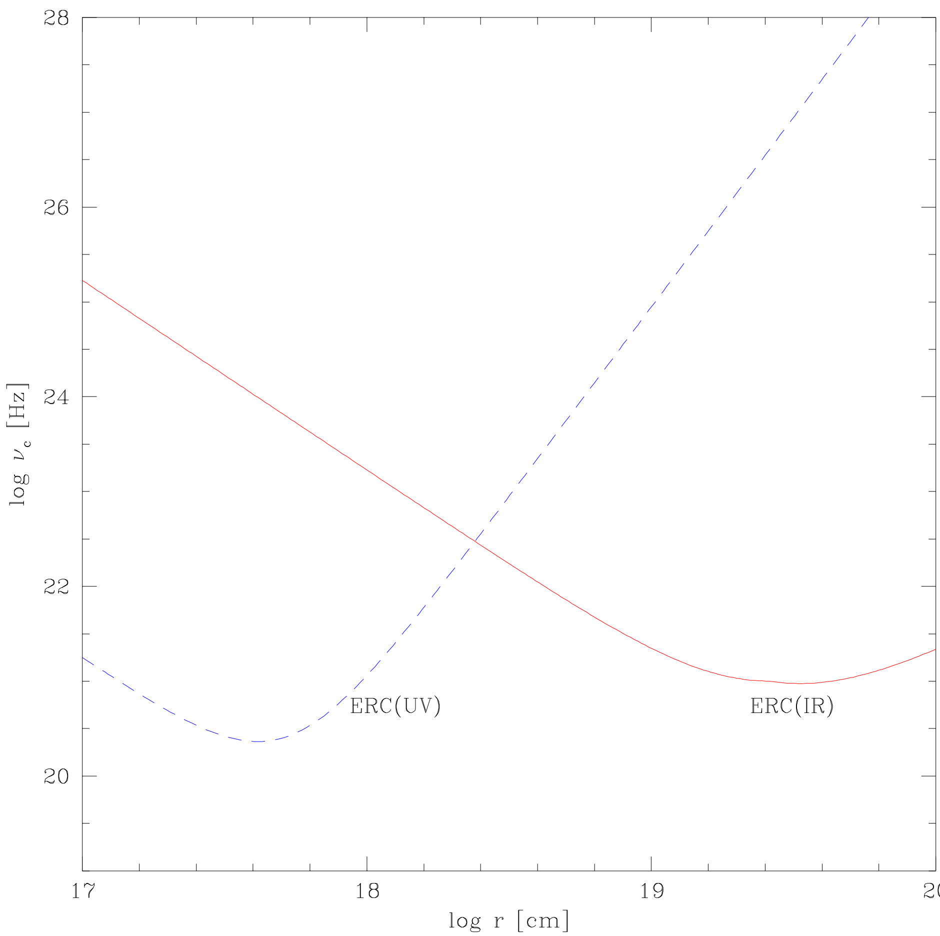
28
26
24
22
20
log ν_c [Hz]
17
18
19
20
log r [cm]
ERC(UV)
ERC(IR)

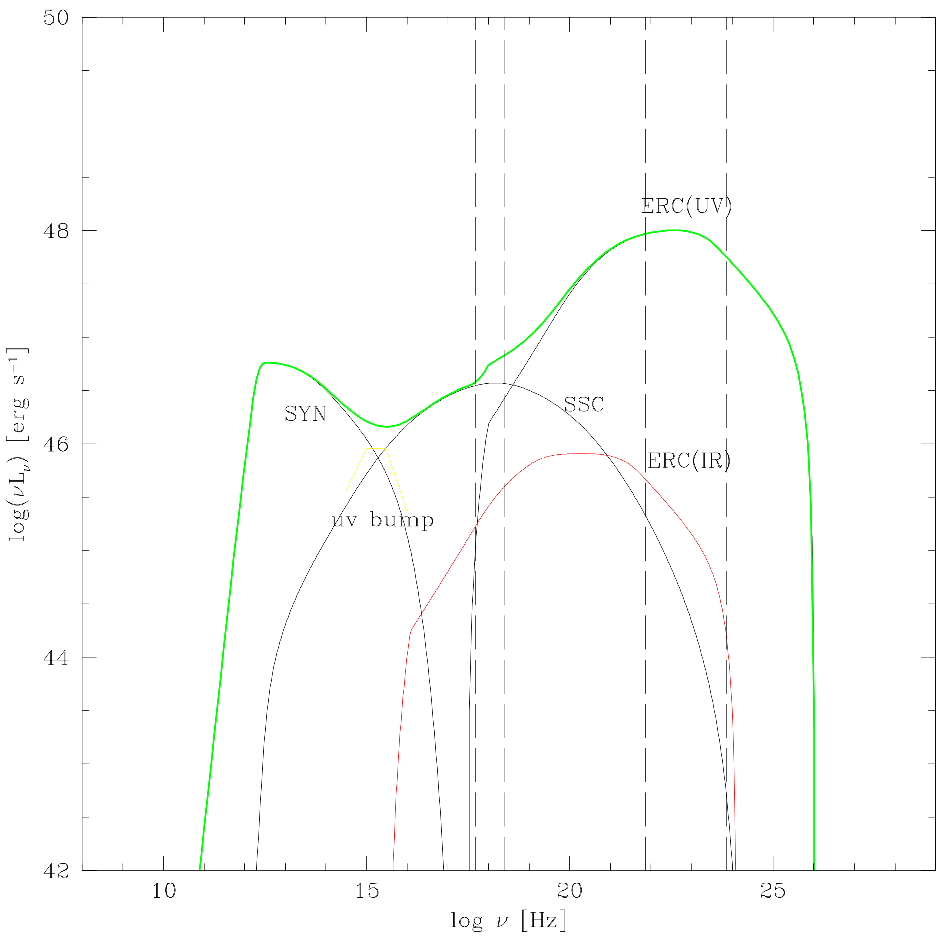
50
48
46
44
42
10
15
20
25
log(νL_ν) [erg s⁻¹]
log ν [Hz]
ERC(UV)
SYN
SSC
ERC(IR)
uv bump

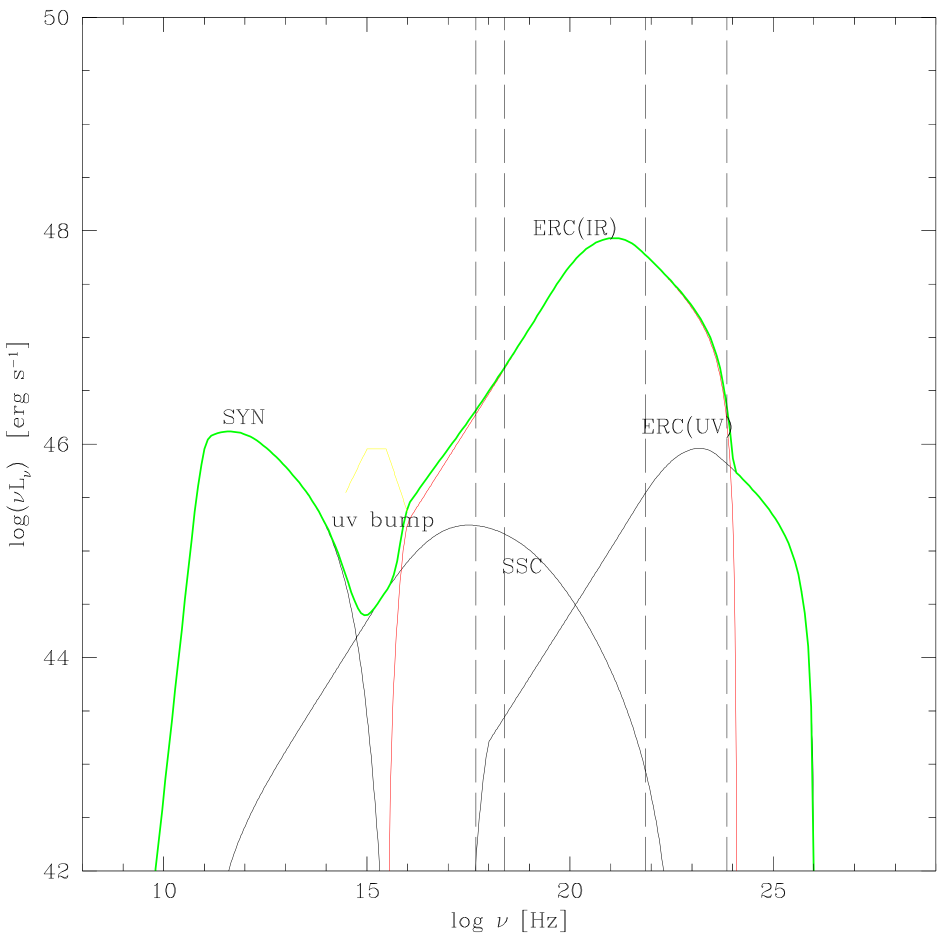

log(νL$_ν$) [erg s^{-1}]
log ν [Hz]
50
48
46
44
42
10
15
20
25
SYN
uv bump
SSC
ERC(IR)
ERC(UV)

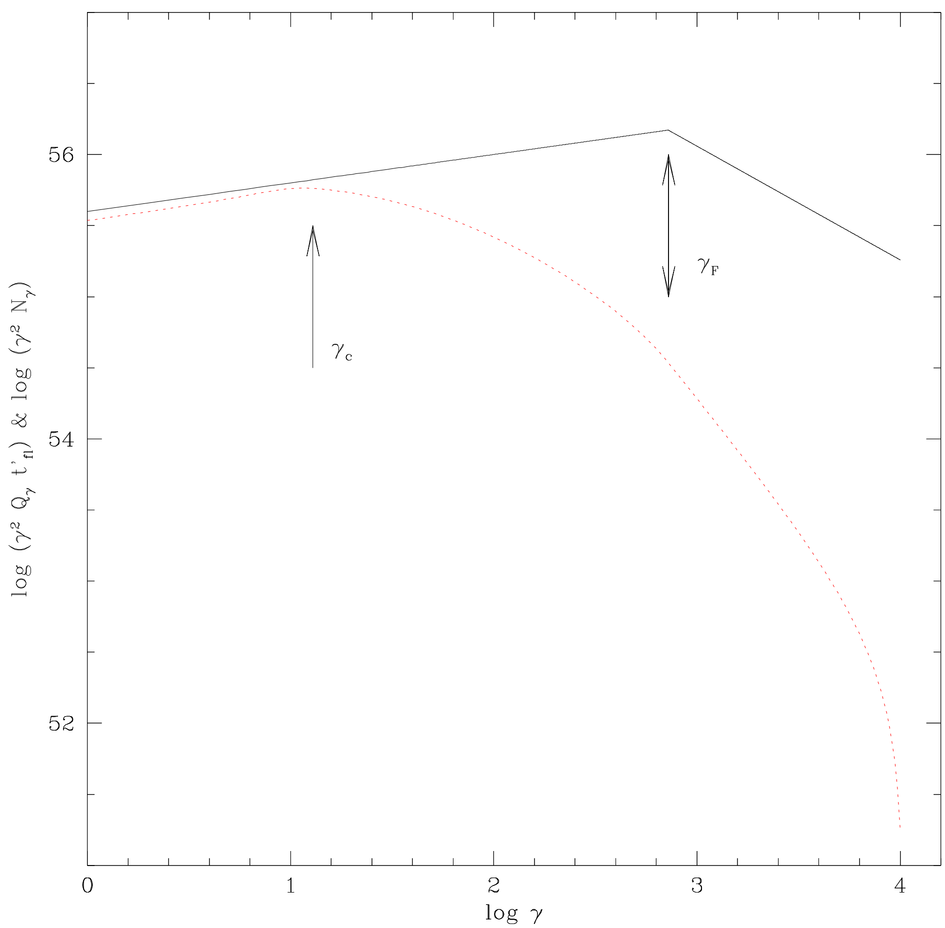

56
54
52
0
1
2
3
4
log γ
log (γ² Q_γ t'_fl) & log (γ² N_γ)
γ_c
γ_F

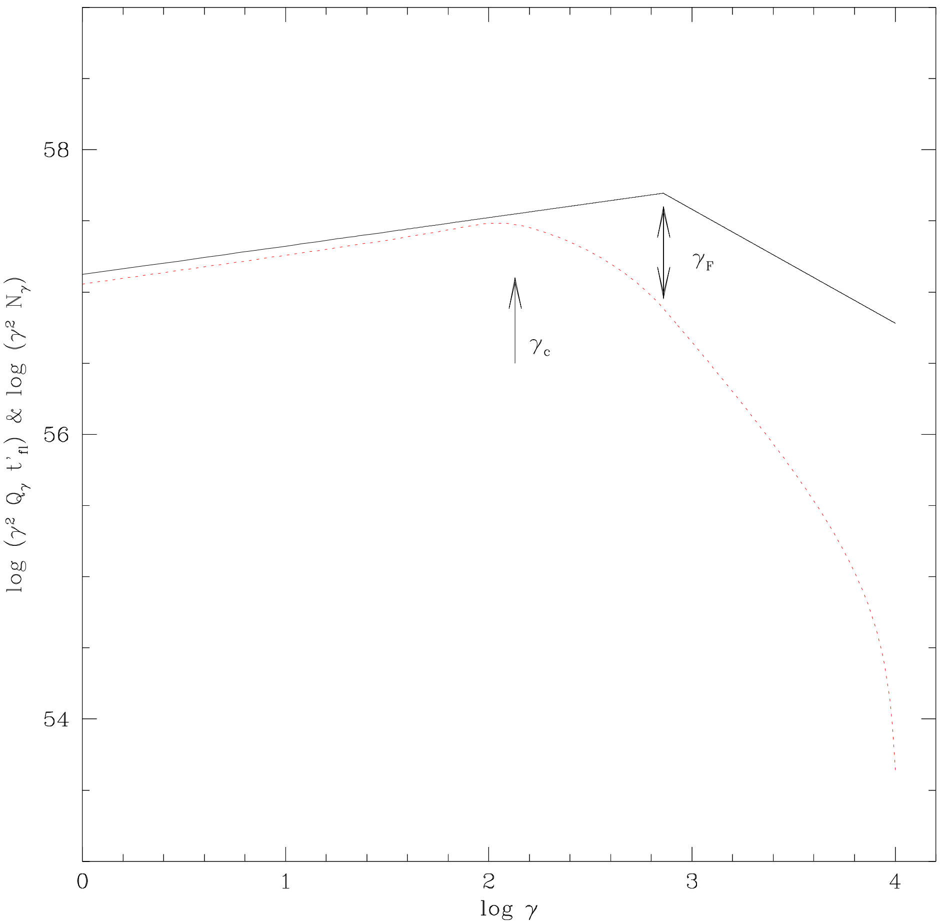
58
56
54
0
1
2
3
4
log γ
log (γ² Q_γ t'_fl) & log (γ² N_γ)
γ_c
γ_F